



Annual Review of Fluid Mechanics

Instabilities of Internal Gravity Wave Beams

Thierry Dauxois, Sylvain Joubaud, Philippe Odier, and Antoine Venaille

Université de Lyon, ENS de Lyon, Université Claude Bernard, CNRS, Laboratoire de Physique, 69342 Lyon, France; email: Thierry.Dauxois@ens-lyon.fr

Annu. Rev. Fluid Mech. 2018. 50:131–56

The *Annual Review of Fluid Mechanics* is online at fluid.annualreviews.org

<https://doi.org/10.1146/annurev-fluid-122316-044539>

Copyright © 2018 by Annual Reviews.
All rights reserved

Keywords

internal waves, mean flow, plane wave solution, internal wave beam, triadic resonant instability, finite-width effect

Abstract

Internal gravity waves play a primary role in geophysical fluids: They contribute significantly to mixing in the ocean, and they redistribute energy and momentum in the middle atmosphere. Until recently, most studies were focused on plane wave solutions. However, these solutions are not a satisfactory description of most geophysical manifestations of internal gravity waves, and it is now recognized that internal wave beams with a confined profile are ubiquitous in the geophysical context. We discuss the reason for the ubiquity of wave beams in stratified fluids, which is related to the fact that they are solutions of the nonlinear governing equations. We focus more specifically on situations with a constant buoyancy frequency. Moreover, in light of recent experimental and analytical studies of internal gravity beams, it is timely to discuss the two main mechanisms of instability for those beams: (a) the triadic resonant instability generating two secondary wave beams and (b) the streaming instability corresponding to the spontaneous generation of a mean flow.



1. INTRODUCTION

Internal gravity waves play a primary role in geophysical fluids (Sutherland 2010): They contribute significantly to mixing in the ocean (Wunsch & Ferrari 2004), and they redistribute energy and momentum in the middle atmosphere (Fritts & Alexander 2003). The generation and propagation mechanisms are fairly well understood, as in the case of oceanic tidal flows (Garrett & Kunze 2007). By contrast, the dissipation mechanisms, together with the understanding of observed energy spectra resulting from nonlinear interactions between those waves, are still debated (Johnston et al. 2003, MacKinnon & Winters 2005, Rainville & Pinkel 2006, Callies et al. 2014, Alford et al. 2015, Sarkar & Scotti 2016). Several routes toward dissipation have been identified, from wave–mean flow interactions to cascade processes, but the contribution of these processes to wave dissipation remains a fairly open subject from both theoretical (Craik 1988, Nazarenko 2011) and experimental (Staquet & Sommeria 2002) points of view. The objective of this review is to present important recent progress that sheds new light on the nonlinear destabilization of internal wave beams, bridging part of the gap between our understanding of their generation mechanisms based mostly on linear analysis and their subsequent evolution through nonlinear effects.

Until recently, most studies were focused on plane wave solutions, which are introduced in classical textbooks (Gill 1982). Strikingly, such plane waves are solutions not only of the linearized dynamics, but also of the nonlinear equations (McEwan 1973, Tabaei & Akylas 2003). However, spatially and temporally monochromatic internal wave trains are not a satisfactory description of most geophysical internal gravity waves (Sutherland 2013). Indeed, oceanic field observations have reported internal gravity beams with a confined profile (Lien & Gregg 2001, Cole et al. 2009, Johnston et al. 2011). In the atmosphere, gravity waves due to thunderstorms also often form beam-like structures (Alexander 2003). Oceanic wave beams arise from the interaction of the barotropic tide with seafloor topography, as has been studied theoretically and numerically (Khaliwala 2003, Lamb 2004, Maugé & Gerkema 2008), taking into account transient, finite-depth, and nonlinear effects ignored in earlier seminal work by Bell (1975). The importance of those beams has also been emphasized in quantitative laboratory experiments (Gostiaux & Dauxois 2007, Peacock et al. 2008, King et al. 2009). From these different works, it is now recognized that internal wave beams are ubiquitous in the geophysical context.

The usual pedagogical introduction to internal waves by oscillating a cylinder in a stratified fluid involves the generation of four wave beams in the pattern of Saint Andrews cross (Mowbray & Rarity 1967). Thorough studies of internal wave beams can be found in Voisin (2003). Moreover, Tabaei & Akylas (2003) have realized that an inviscid uniformly stratified Boussinesq fluid supports time-harmonic plane waves invariant in one transverse-horizontal direction, propagating along a direction determined by the ratio between the oscillating frequency and the buoyancy frequency, with a general spatial profile in the cross-beam direction. These wave beams not only are fundamental to the linearized dynamics, but also happen to be, like sinusoidal wave trains, exact solutions of the nonlinear governing equations. Remarkably, Tabaei & Akylas (2003) showed that the steady-state similarity linear solution for a viscous beam (Thomas & Stevenson 1972) is also valid in the nonlinear regime. In light of the recent experimental and analytical studies of those internal gravity wave beams, it is a good time to study their stability properties.

In the next section, we introduce the subject by presenting concepts, governing equations, and approximations that lead to the description of gravity waves in stratified fluids. We place special emphasis on the peculiar role of nonlinearities in explaining why internal gravity wave beams are ubiquitous solutions in oceans and middle atmospheres. Then, in Section 3, we discuss the classic triadic resonant instability (TRI) that corresponds to the destabilization of a primary wave with the spontaneous emission of two secondary waves of lower frequencies and with different wave



vectors. In addition to the simple case of plane waves, we discuss in detail the generalization to wave beams with a finite width. Section 4 is dedicated to the streaming instability, the second important mechanism for the instability of internal gravity waves beams through the generation of a mean flow. Finally, in Section 5, we draw some conclusions and discuss future issues.

2. THE DYNAMICS OF STRATIFIED FLUIDS AND THEIR SOLUTIONS

2.1. Basic Equations

Consider an incompressible, nonrotating, stratified Boussinesq fluid in Cartesian coordinates $(\mathbf{e}_x, \mathbf{e}_y, \mathbf{e}_z)$, where \mathbf{e}_z is the direction opposite of gravity. The Boussinesq approximation amounts to neglecting density variations with respect to a constant reference density ρ_{ref} , except when those variations are associated with the gravity term g . The relevant field to describe the effect of density variations is then the buoyancy field $b_{\text{tot}} = g(\rho_{\text{ref}} - \rho) / \rho_{\text{ref}}$, where $\rho(\mathbf{r}, t)$ is the full density field, $\mathbf{r} = (x, y, z)$ is the spatial coordinate, and t is the time coordinate. Let $\rho_0(z)$ be the density of the flow at rest, with buoyancy frequency $N(z) = (-g(\partial_z \rho_0) / \rho_{\text{ref}})^{1/2}$. The corresponding buoyancy profile $g(\rho_{\text{ref}} - \rho_0) / \rho_{\text{ref}}$ is denoted b_0 . The buoyancy frequency N varies in principle with the depth z . In the ocean, N is rather large in the thermocline and weaker in the abyss. However, for simplicity, in the rest of the review N is taken to be constant. To greatly simplify the theoretical analysis, one can relax this approximation (which looks drastic at first sight) when N changes smoothly by relying on the Wentzel–Kramers–Brillouin approximation.

The equations of motion can be written as a dynamical system for the perturbed buoyancy field $b = b_{\text{tot}} - b_0$ and the three components of the velocity field $\mathbf{u} = (u_x, u_y, u_z)$:

$$\nabla \cdot \mathbf{u} = 0, \tag{1}$$

$$\partial_t \mathbf{u} + \mathbf{u} \cdot \nabla \mathbf{u} = -\frac{1}{\rho_{\text{ref}}} \nabla p + b \mathbf{e}_z + \nu \nabla^2 \mathbf{u}, \tag{2}$$

$$\partial_t b + \mathbf{u} \cdot \nabla b + u_z N^2 = 0, \tag{3}$$

where $p(\mathbf{r}, t)$ is the pressure variation with respect to the hydrostatic equilibrium pressure $P_0(z) = P_0(0) - \int_0^z \rho_0(z')g \, dz'$ and ν is the kinematic viscosity. We have neglected the molecular diffusivity, which would imply a term $D\nabla^2 b$ on the right-hand side of Equation 3, where D is the diffusion coefficient of the stratifying element (molecular diffusivity for salt, thermal diffusivity for temperature). The importance of the dissipative terms with respect to the nonlinear ones is described by the Reynolds UL/ν and the Peclet numbers UL/D (where U and L are typical velocity and length scales) or, equivalently, by the Reynolds number and the Schmidt number ν/D . In many geophysical situations, both the Reynolds and the Peclet numbers are large, and molecular effects can be neglected at the lowest order. In such cases, the results do not depend on the Schmidt number. In laboratory settings, the Peclet number is often also very large, at least when the stratification agent is salt, in which case $D \approx 10^{-9} \text{ m}^2/\text{s}$. However, the viscosity of water is $\nu \approx 10^{-6} \text{ m}^2/\text{s}$, and the corresponding Reynolds numbers are such that viscous effects can play an important role, as seen below.

Let us first consider the simplest case of two-dimensional (2D) flow, which is invariant in the transverse y direction. The nondivergent 2D velocity field is then conveniently expressed in terms of a stream function $\psi(x, z)$ as $\mathbf{u} = (\partial_z \psi, 0, -\partial_x \psi)$. Introducing the Jacobian $J(\psi, b) = \partial_x \psi \partial_z b - \partial_x b \partial_z \psi$, the dynamical system of Equations 1–3 is expressed as

$$\partial_t \nabla^2 \psi + J(\nabla^2 \psi, \psi) = -\partial_x b + \nu \nabla^4 \psi, \tag{4}$$

$$\partial_t b + J(b, \psi) - N^2 \partial_x \psi = 0. \tag{5}$$



Plane wave:

$\psi_0 e^{i(\mathbf{k}\cdot\mathbf{r}-\omega t)}$ + c.c.,
 where c.c. denotes the complex conjugate

Differentiating Equation 4 with respect to time and Equation 5 with respect to the spatial variable x , and subtracting the latter from the former, one gets finally

$$\partial_{tt}\nabla^2\psi + N^2\partial_{xx}\psi = \nu\nabla^4\psi + \partial_t J(\psi, \nabla^2\psi) + \partial_x J(b, \psi), \tag{6}$$

which describes the nonlinear dynamics of nonrotating, nondiffusive viscous stratified fluids in two dimensions.

2.2. Linear Approximation

In the linear approximation, assuming vanishing viscosity, the right-hand side of Equation 6 immediately vanishes, leading to the following wave equation for the stream function:

$$\partial_{tt}\nabla^2\psi + N^2\partial_{xx}\psi = 0. \tag{7}$$

This equation is striking for several reasons. First, its mathematical structure is clearly different from the traditional d'Alembert equation. Indeed, the spatial differentiation appears at second order in both terms. Time-harmonic plane waves with frequency ω , wave vector $\mathbf{k} = (\ell, 0, m)$, and wave number $k = |\mathbf{k}| = (\ell^2 + m^2)^{1/2}$ are solutions of Equation 7 if the dispersion relation for internal gravity waves,

$$\omega = \pm N \frac{\ell}{k} = \pm N \sin \theta, \tag{8}$$

is satisfied, where θ is the angle between the wave number \mathbf{k} and the vertical.

Second, contrary to the usual concentric waves emitted from the source of excitation when considering the d'Alembert equation, here four different directions of propagation are possible depending on the sign of ℓ and m . This is an illustration of the anisotropic propagation due to the vertical stratification.

Third, the dispersion relation features the angle of propagation rather than the wave length, emphasizing a clear difference between internal waves and surface waves. This is also a crucial property for this review, because it allows us to define beams with a general profile, rather than with a single wave number.

2.3. Nonlinear Terms

Let us consider now the modification introduced by the nonlinear terms of Equation 6: first for internal plane wave solutions and then for internal wave beams.

2.3.1. Plane wave solutions. It is striking and pretty unusual that plane waves are solutions of the inviscid nonlinear Equation 6 even for large amplitudes. Indeed, the stream function of the plane wave solution is a Laplacian eigenmode, with $\nabla^2\psi = -k^2\psi$. Consequently, the first Jacobian term vanishes in Equation 6. Equation 4 leads therefore to the so-called polarization relation $b = -(N^2\ell/\omega)\psi \equiv \mathcal{P}\psi$, where \mathcal{P} is the polarization prefactor. Consequently, the second Jacobian in Equation 6 vanishes: $J(\psi, \mathcal{P}\psi) = 0$. To conclude, both nonlinear terms in Equation 6 vanish for plane wave solutions, which are therefore solutions of the nonlinear equation for any amplitude.

2.3.2. Internal wave beams. Because the frequency ω is independent of the wave number, it is possible to devise more general solutions, time harmonic with the same frequency ω , by superposing several linear solutions associated with the same angle of propagation, but with different wave numbers k (McEwan 1973, Tabaei & Akylas 2003). Introducing the along-beam coordinate $\xi = x \cos \theta - z \sin \theta$, defined along the direction of propagation, and the cross-beam coordinate



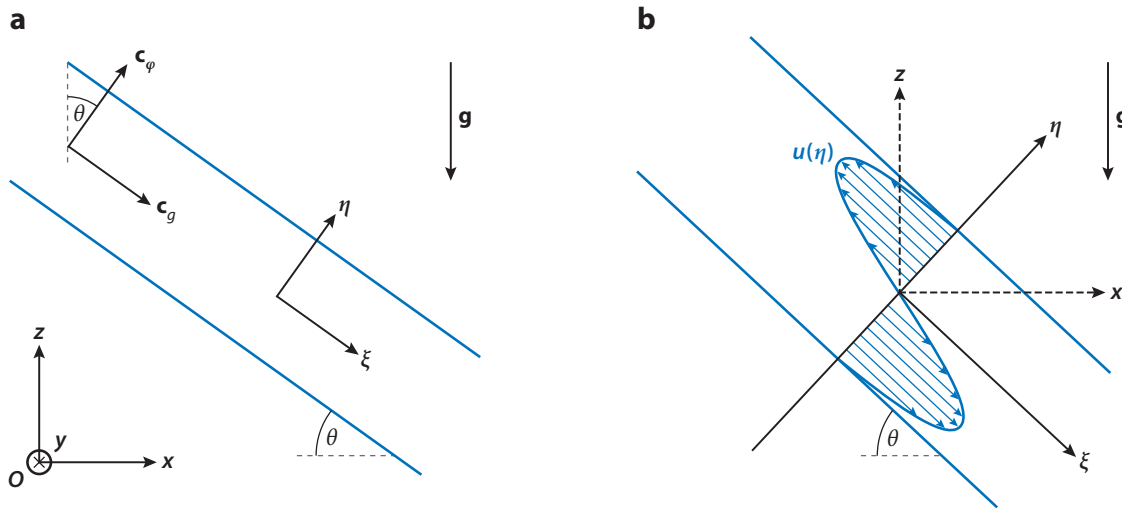


Figure 1

(a) Schematic representation of an internal wave beam and definition of the longitudinal ξ and cross-beam η coordinates, the angle of inclination θ , and the group \mathbf{c}_g and phase \mathbf{c}_ϕ velocities. (b) Geometry of a uniform (along ξ) internal wave beam inclined at an angle θ with respect to the horizontal. The beam profile varies in the cross-beam η direction, and the associated flow velocity is in the along-beam direction ξ . The transverse-horizontal direction is denoted by y and gravity is denoted by \mathbf{g} .

$\eta = x \sin \theta + z \cos \theta$ (Figure 1), one can write the plane wave solution as

$$\psi(x, y, z, t) = \psi_0 e^{i(\ell x + m z - \omega t)} + \text{c.c.} = \psi_0 e^{ik\eta} e^{-i\omega t} + \text{c.c.}, \tag{9}$$

given that $\ell = k \sin \theta$ and $m = k \cos \theta$, where c.c. denotes the complex conjugate. By introducing $Q(\eta) = ik\psi_0 e^{ik\eta}$, one obtains the velocity field $\mathbf{u} = Q(\eta)(\cos \theta, 0, -\sin \theta)e^{-i\omega t} + \text{c.c.}$ and the buoyancy perturbation $b = -i(\mathcal{P}/k)Q(\eta)e^{-i\omega t} + \text{c.c.}$

One can actually obtain a wider class of solutions by considering an arbitrary complex amplitude $Q(\eta)$. Indeed, the fields \mathbf{u} and b do not depend on the longitudinal variable ξ . Consequently, after the change of variables, the Jacobian $J(\psi, b) = \partial_\xi \psi \partial_\eta b - \partial_\xi b \partial_\eta \psi$ simply vanishes, making the governing equations linear. As discussed by Tabaei et al. (2005), unidirectional beams, in which energy propagates in one direction, involve plane waves with wave numbers of the same sign only: $Q(\eta) = \int_0^{+\infty} A(k)e^{ik\eta} dk$ or $Q(\eta) = \int_{-\infty}^0 A(k)e^{ik\eta} dk$.

The class of propagating waves that are solutions of the nonlinear dynamics in a Boussinesq stratified fluid is much more general than plane wave solutions: There is a whole family of solutions corresponding to uniform plane waves in the longitudinal direction ξ , but with a general profile in the cross-beam direction η , as represented in Figure 1.

Tabaei & Akylas (2003) have generalized those results by computing asymptotic solutions for a slightly viscous, nonlinear wave beam with amplitude slowly modulated along ξ and in time. After considerable manipulation, it turns out that all leading-order, nonlinear, advective acceleration terms in the governing equations of motion vanish, and a uniform (along ξ) beam, regardless of its profile (along η), represents an exact nonlinear solution in an unbounded, inviscid, uniformly stratified fluid. This result not only extends the validity of the Thomas & Stevenson (1972) steady-state similarity solution to the nonlinear regime, but also emphasizes how nonlinearity has only relatively weak consequences. This has profound and useful outcomes for the applicability of results obtained with linear theory when one wants to compare with field observations, laboratory experiments, or numerical simulations.

Internal wave beam:

superposition of time-harmonic plane waves with an arbitrary profile in the cross-beam direction; we will call uniform beam the special case of an internal plane wave with a confined spatial profile



The vanishing of the nonlinear contributions is unexpected and results from the combination of numerous different terms. Tabaei & Akylas (2003) noticed, however, that the underlying reason for the seemingly miraculous cancelation of the resonant nonlinear terms was the same one Dauxois & Young (1999) already pointed out. After lengthy calculations, in both cases, the reason is a special case of the Jacobi identity $J[A, J(B, C)] + J[C, J(A, B)] + J[J(A, C), B] = 0$. Dauxois & Young (1999) were studying near-critical reflection of a finite-amplitude internal wave on a slope, in order to heal the singularity occurring in Phillips' (1966) solution. Using a matched asymptotic, they took a distinguished limit in which the amplitude of the incident wave, the dissipation, and the departure from criticality are all small. In the end, although the reconstructed fields do contain nonlinearly driven second harmonics, they obtained the striking result that the final amplitude equation happens to be a linear equation. The underlying reason was already this Jacobi identity. [Studying the mechanism of superharmonic generation, Liang et al. (2017) recently reported another situation for which the nonlinear terms vanish in the domain bulk. Interestingly, however, they play a pivotal role through the free surface boundary condition.]

To conclude, the effects of nonlinearities on plane waves or wave beams exhibit very peculiar properties. There are two important points to keep in mind. First, plane waves and internal wave beams are solutions of the full equation. Second, identifying a solution does not mean that it is a stable one. This remark is at the core of the present review: In what follows, we focus on the behavior of wave beams with respect to the TRI and the streaming instability.

3. TRIADIC RESONANT INSTABILITY

3.1. Introduction

It was first realized 50 years ago that internal gravity plane waves are unstable to infinitesimal perturbations, which grow to form temporal and spatial resonant triads (Davis & Acrivos 1967, McEwan 1971, Mied 1976). This nonlinear instability produces two secondary waves that extract energy from a primary one. Energy transfer rates due to this instability are now well established for plane waves (Staquet & Sommeria 2002).

The instability was observed in several laboratory experiments (Benielli & Sommeria 1998, Clark & Sutherland 2010, Pairaud et al. 2010, Joubaud et al. 2012) and numerical experiments on propagating internal waves (Koudella & Staquet 2006; A.F. Wienkers, C. Brouzet & T. Dauxois, unpublished manuscript) or reflecting internal tides on a horizontal or sloping boundary (Gerkema et al. 2006, Pairaud et al. 2010, Zhou & Diamessis 2013, Chalamalla & Sarkar 2016) or at the reflection on a pycnocline (Gayen & Sarkar 2013). Oceanic field observations have also confirmed the importance of this instability, especially close to the critical latitude, where the Coriolis frequency is half of the tidal frequency (Hibiya et al. 2002, MacKinnon et al. 2013, Sun & Pinkel 2013).

However, recent experiments (Bourget et al. 2013) followed by a simple model and numerical simulations (Bourget et al. 2014), as well as a theory by Karimi & Akylas (2014), have shown that finite-width internal gravity wave beams exhibit much more complex behavior than is expected for interacting plane waves. This is discussed below.

3.2. The Simplest Case of Plane Wave Solutions

Let us first consider the case of internal plane wave solutions.

3.2.1. Derivation of the equations and plane wave solutions. Looking for solutions of the basic Equations 4 and 5 as a sum of three plane waves, where $b = \sum_j R_j(t) e^{i(\mathbf{k}_j \cdot \mathbf{r} - \omega_j t)} + \text{c.c.}$,



$\psi = \sum_j \Psi_j(t) e^{i(\mathbf{k}_j \cdot \mathbf{r} - \omega_j t)} + \text{c.c.}$, $j = 0$ for the primary wave, and $j = \pm$ for the secondary ones, one gets (e.g., see Hasselman 1967)

$$\sum_j [-k_j^2 (\dot{\Psi}_j - i\omega_j \Psi_j) + i\ell_j R_j - \nu k_j^4 \Psi_j] e^{i(\mathbf{k}_j \cdot \mathbf{r} - \omega_j t)} + \text{c.c.} = -J(\nabla^2 \psi, \psi), \quad 10.$$

$$\sum_j (\dot{R}_j - i\omega_j R_j - iN^2 \ell_j \Psi_j) e^{i(\mathbf{k}_j \cdot \mathbf{r} - \omega_j t)} + \text{c.c.} = -J(b, \psi), \quad 11.$$

where \dot{R} is the derivative of the amplitude R . The left-hand sides represent the linear parts of the dynamics. Neglecting the nonlinear terms, the viscous terms, and the temporal evolution of the amplitudes, one recovers the polarization expression $R_j = -(N^2 \ell_j / \omega_j) \Psi_j$ and the dispersion relation $\omega_j = N |\ell_j| / \sqrt{\ell_j^2 + m_j^2}$. This linear system is resonantly forced by the Jacobian nonlinear terms on the right-hand side when the waves fulfill a spatial resonance condition,

$$\mathbf{k}_0 = \mathbf{k}_+ + \mathbf{k}_-, \quad 12.$$

and a temporal resonance condition,

$$\omega_0 = \omega_+ + \omega_-. \quad 13.$$

The Jacobian terms in Equations 10 and 11 can then be written as the sum of a resonant term that will drive the instability and some unimportant nonresonant terms. Introducing this result into Equation 10, one obtains three relations between Ψ_j and R_j for each mode $\exp[i(\mathbf{k}_j \cdot \mathbf{r} - \omega_j t)]$, with $j = 0, +$, or $-$:

$$R_{\pm} = \frac{1}{i\ell_{\pm}} [k_{\pm}^2 (\dot{\Psi}_{\pm} - i\omega_{\pm} \Psi_{\pm}) + \nu k_{\pm}^4 \Psi_{\pm} + \alpha_{\pm} \Psi_0 \Psi_{\mp}^*], \quad 14.$$

where $\alpha_{\pm} = (\ell_0 m_{\mp} - m_0 \ell_{\mp})(k_0^2 - k_{\mp}^2)$. Here, one traditionally uses the so-called pump-wave approximation, which assumes that, over the initial critical growth period of the secondary waves, the primary wave amplitude Ψ_0 remains constant and that the amplitude varies slowly with respect to the period of the wave ($\dot{\Psi}_j \ll \omega_j \Psi_j$). Differentiating the polarization expression, cumbersome but straightforward calculations (Bourget et al. 2013) lead, to the first order of approximation, to

$$\frac{d\Psi_{\pm}}{dt} = |I_{\pm}| \Psi_0 \Psi_{\mp}^* - \frac{\nu}{2} k_{\pm}^2 \Psi_{\pm}, \quad 15.$$

where $I_{\pm} = (\ell_0 m_{\mp} - m_0 \ell_{\mp})[\omega_{\pm}(k_0^2 - k_{\mp}^2) + \ell_{\pm} N^2 (\ell_0 / \omega_0 - \ell_{\mp} / \omega_{\mp})] / (2\omega_{\pm} k_{\pm}^2)$.

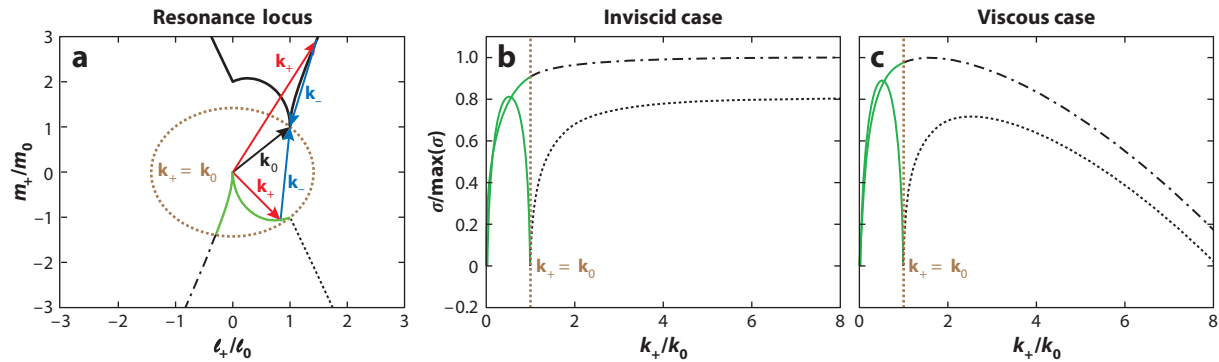
Differentiating Equation 15, one gets

$$\ddot{\Psi}_{\pm} = I_+ I_- |\Psi_0|^2 \Psi_{\pm} - \frac{\nu^2}{4} k_+^2 k_-^2 \Psi_{\pm} - \frac{\nu}{2} (k_+^2 + k_-^2) \dot{\Psi}_{\pm}. \quad 16.$$

The general solution is $\Psi_{\pm}(t) = A_{1,2} \exp(\sigma t) + B_{1,2} \exp(\sigma' t)$, where $\sigma = -\nu(k_+^2 + k_-^2)/4 + \sqrt{(v/4)^2 (k_+^2 - k_-^2)^2 + I_+ I_- |\Psi_0|^2}$ and $\sigma' < 0 < \sigma$.

In conclusion, a vanishingly small-amplitude noise induces the growth of two secondary waves by a triadic resonant mechanism. Because their sum gives the primary frequency (see Equation 13), ω_+ and ω_- are subharmonic waves. The growth rate of the instability depends on the characteristics of the primary wave, namely, its wave vector, its frequency, and its amplitude Ψ_0 , but also on the viscosity ν .




Figure 2

(a) Resonance locus for the unstable wave vectors (ℓ_+, m_+) satisfying Equation 17 once the primary wave vector $\mathbf{k}_0 = (\ell_0, m_0)$ is given. The central (green lines) and external (solid, dashed, and dotted-dashed black lines) branches are shown. The dotted brown curve is defined by $k_+ = k_0$. Two examples of vector triads $(\mathbf{k}_0, \mathbf{k}_+, \mathbf{k}_-)$ are shown. (b,c) Growth rates $\sigma/\max(\sigma)$, corresponding to the different branches, as a function of the normalized wave vector modulus k_+/k_0 . Panel b presents the inviscid case, whereas panel c presents a viscous case corresponding to $\Psi_0/\nu = 100$. The growth rate corresponding to the solid black line in panel a is not plotted in panels b and c to emphasize the transition from small to large scales. One can recover it using the symmetry $\mathbf{k} \rightarrow \mathbf{k}_0 - \mathbf{k}$ discussed in Section 3.2.2.

3.2.2. Triads, resonance loci, and growth rates. With the dispersion relation for internal waves, the temporal resonance condition leads to (Bourget et al. 2013)

$$\frac{|\ell_0|}{\sqrt{\ell_0^2 + m_0^2}} = \frac{|\ell_+|}{\sqrt{\ell_+^2 + m_+^2}} + \frac{|\ell_0 - \ell_+|}{\sqrt{(\ell_0 - \ell_+)^2 + (m_0 - m_+)^2}}, \quad 17.$$

whose solutions are presented in **Figure 2a**. Once the primary wave vector \mathbf{k}_0 is defined, any point of the solid curve corresponds to the tip of the \mathbf{k}_+ vector, and \mathbf{k}_- is obtained by closing the triangle. The choice between the labels + and - is essentially arbitrary, and this leads to the symmetry $\mathbf{k} \rightarrow \mathbf{k}_0 - \mathbf{k}$ in **Figure 2a**. Without loss of generality, we always call \mathbf{k}_+ the largest wave number.

One can observe two distinct parts of this resonance locus, characterized by the position of k_+/k_0 with respect to unity. The wavelengths of the secondary waves generated by the instability can be both smaller than the primary wavelength, or one can be larger and the other smaller. The former case corresponds to the external branch of the resonance locus and implies an energy transfer toward smaller scales. The latter case corresponds to the central branch of the resonance locus and implies an energy transfer toward smaller and larger scales.

Among the different possible solutions on the resonance locus, the one expected to be seen experimentally or numerically is the one associated with the largest growth rate. In the inviscid case, the most unstable growth rate occurs for $k \rightarrow \infty$, with essentially $\mathbf{k}_+ \approx -\mathbf{k}_-$ and therefore $\omega_+ = \omega_- = \omega_0/2$. This ultraviolet catastrophe is healed in the presence of viscosity, which selects a finite wavelength for the maximum growth rate (**Figure 2c**) (Hazewinkel & Winters 2011). For typical laboratory-scale experiments, the values of k_+ corresponding to significant growth rates are of the same order of magnitude as the primary wave number k_0 , as can be seen in **Figure 2c**, with $k_-/k_0 \approx 1.5$ and $k_+/k_0 \approx 2.3$. Thus, the TRI corresponds to a direct energy transfer from the primary wave to small scales where viscous effects come into play, without the need for a turbulent cascade process.

The fact that viscosity has a significant effect on the selection of the excited resonant triad, preventing any large-wave number secondary wave to grow from the instability, has been observed

in laboratory experiments on wave beams (Bourget et al. 2013). However, Bourget et al. (2013) also found a type of triad different from those predicted by previous theoretical arguments, as discussed in the following sections.

3.2.3. Amplitude threshold for plane wave solutions. The expression for the growth rate σ implies that the amplitude of the stream function has to be larger than the critical value $|\Psi_c(\ell_+, m_+)| = \nu k_+ k_- / \sqrt{4I_+ I_-}$ in order for there to be a strictly positive growth rate (Koudella & Staquet 2006, Bourget et al. 2013). The threshold for the instability is thus given by the global minimum of this function of several variables. Let us focus on the particular case where \mathbf{k}_+ tends to \mathbf{k}_0 by considering the following description of the wave vector components $\ell_+ = \ell_0(1 + \mu_0 \varepsilon^\alpha)$ and $m_+ = m_0(1 + \varepsilon)$, where $0 < \varepsilon \ll 1$, $\alpha \geq 1$, and $\mu_0 > 0$. Using the dispersion relation and the temporal and spatial resonance conditions, Bourget et al. (2014) have shown that $\alpha = 2$ is the only acceptable value to balance the lowest-order terms. Plugging these relations into the expression of I_\pm , one gets $I_+ = -\ell_0 m_0 \varepsilon + o(\varepsilon)$ and $I_- = -\ell_0 m_0 + o(1)$, which leads to $|\Psi_c| = \sqrt{\varepsilon} \nu N / (2\omega_0) + o(\varepsilon^{1/2})$. Because this positive expression's minimum is zero, there is no threshold for an infinitely wide wave beam, even when considering a viscous fluid. Plane wave solutions are thus always unstable to this TRI.

3.3. Why Does the Finite Width of Internal Wave Beams Matter?

The above theory for the TRI does not take into account the finite width of the experimental beam. Qualitatively, the subharmonic waves can only extract energy from the primary wave if they do not leave the primary beam before they extract substantial energy (Bourget et al. 2014). The group velocity of the primary wave is aligned with the beam, but the group velocity of the secondary waves is definitely not aligned, and these secondary waves eventually leave the primary wave beam (Figure 3). This is a direct consequence of the dispersion relation, which relates the direction of propagation to the frequency: A different frequency, smaller for subharmonic waves, will lead to a shallower angle.

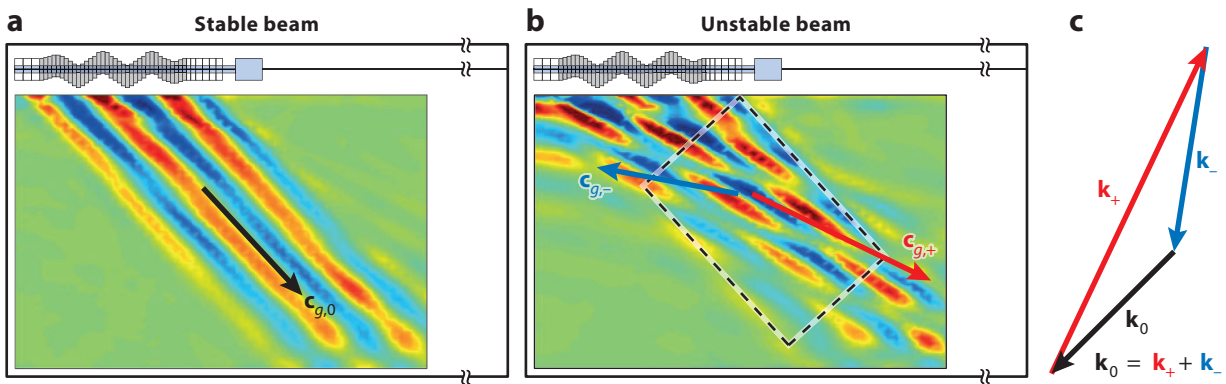


Figure 3

Sketch of the experimental setup (Bourget et al. 2013), showing the wave generator lying horizontally at the top of the wave tank with a superimposed snapshot of the vertical density gradient field. (a) The internal wave beam propagating downward. (b) The instability of the propagating internal wave beam, with a control area for the energy approach (dashed black rectangle) (Bourget 2014). (c) The vector triad comprising the primary wave vector \mathbf{k}_0 (black) and the two secondary waves vectors \mathbf{k}_+ (red) and \mathbf{k}_- (blue). From this triad, it is possible to deduce the orientation of the group velocities of the three different waves as shown in panels a and b.



Three comments are in order. First, the angles between primary and secondary waves strongly influence the interaction time and thus the instability.

Second, having a larger group velocity $c_{g,\pm} = (N^2 - \omega_{\pm}^2)^{1/2} / k_{\pm}$, secondary waves with small wave vectors leave the primary wave beam more rapidly and have less time to grow in amplitude. Such solutions will therefore be less likely to develop, opening the door to stabilization of the primary wave by the finite-width effect. This clarifies why experiments with the most unstable secondary waves on the internal branch (small wave vector case) of the resonance locus (**Figure 3**) were found to be stable (Bourget et al. 2013), contrary to the prediction for plane waves. McEwan & Plumb (1977) long ago identified this decisive role of the short-scale subharmonic waves' group velocity.

Third, at the other end of the spectrum, small wavelengths are more affected by dissipation and will also be less likely to be produced by TRI. Consequently, only a window of secondary wavelengths is possibly produced by TRI.

3.4. Energy Approach

A simple energy balance proposed by Bourget et al. (2014) allows for an insightful and more quantitative estimate for the most unstable triad. We introduce a control area in **Figure 3b** (denoting the perpendicular beam width W), and we neglect the spatial attenuation of the primary wave in this region (the pump-wave approximation). Because secondary waves do not propagate parallel to the primary beam, they exit the control area from the lateral boundaries without compensation. Equation 15 is thus modified as follows:

$$\frac{d\Psi_{\pm}}{dt} = |I_{\pm}| \Psi_0 \Psi_{\mp}^* - \frac{\nu}{2} k_{\pm}^2 \Psi_{\pm} - \frac{|\mathbf{c}_{g,\pm} \cdot \mathbf{e}_{k_0}|}{2W} \Psi_{\pm}. \quad 18.$$

The first term represents the interaction with the other plane waves of the triadic resonance, the second term is due to viscous damping, and the third accounts for the energy leaving the control area.

One also finds here exponentially growing solutions with a positive growth rate slightly modified as $\sigma^* = -(\Sigma_+ + \Sigma_-)/4 + \sqrt{(\Sigma_+ - \Sigma_-)^2/16 + |I_+||I_-||\Psi_0|^2}$, in which the effective viscous term now reads $\Sigma_{\pm} = \nu k_{\pm}^2 + |\mathbf{c}_{g,\pm} \cdot \mathbf{e}_{k_0}|/W$. The finite width of the beam is responsible for a new term characterizing the transport of the secondary wave energy out of the interaction region. For infinitely wide wave beams ($W \rightarrow +\infty$), one recovers the growth rate σ obtained in the plane wave case. In contrast, when the beam becomes narrow ($W \rightarrow 0$), the growth rate decreases to zero, leading to a stabilization.

The finite width of a wave beam therefore increases its stability, owing to the transport of the secondary waves out of the triadic interaction zone of the primary wave beam before they can extract substantial energy. This interaction time scales directly with the perpendicular beam width W as can be seen from the expression of σ^* .

3.5. Theory in the Nearly Inviscid Limit

Recently, Karimi & Akylas (2014) have proposed a beautiful weakly nonlinear asymptotic analysis of the finite-width effect on TRI. Mostly interested in oceanic applications, Karimi & Akylas (2014) looked for subharmonic perturbations in the form of fine-scale, nearly monochromatic wave packets with frequencies close to one-half of the primary frequency. In this limit, usually called parametric subharmonic instability (PSI) (see the sidebar titled The Triadic Resonant Instability Versus



THE TRIADIC RESONANT INSTABILITY VERSUS THE PARAMETRIC SUBHARMONIC INSTABILITY

The classic TRI corresponds to the destabilization of a primary wave through the spontaneous emission of two secondary waves. The frequencies and wave vectors of these three waves are related by the spatial, $\mathbf{k}_0 = \mathbf{k}_+ + \mathbf{k}_-$, and the temporal, $\omega_0 = \omega_+ + \omega_-$, resonance conditions, where the indices 0 and \pm refer to the primary and secondary waves, respectively.

In the inviscid case, the most unstable triad corresponds to antiparallel, infinitely long secondary wave vectors associated with frequencies that are both half of the primary wave frequency: $\omega_+ \approx \omega_- \approx \omega_0/2$. Because of the direct analogy with the parametric oscillator, this particular case defines the parametric subharmonic instability (PSI). This special case applies to many geophysical situations, especially oceanic applications.

In laboratory experiments, viscosity plays an important role, and the two secondary wave frequencies differ. By abuse of language, authors have sometimes used the name PSI to refer to cases for which secondary waves do not oscillate at half the forcing frequency. To avoid confusion, in the general case, it is presumably more appropriate to use the acronym TRI.

the Parametric Subharmonic Instability), ω_{\pm} is approximately $\omega_0/2 = N(\sin \theta)/2 = N \sin \phi$, which defines, with respect to the vertical, the angle ϕ of the wave vectors \mathbf{k}_{\pm} .

The key ingredient in the analytical derivation is to take advantage of the scale difference between the width of the primary beam W and the very small carrier wavelength of the subharmonic wave packets $\lambda_{\pm} = 2\pi/k_{\pm}$. The small-amplitude expansion is thus characterized by the small parameter $\mu = \lambda_{\pm}/(2\pi W)$. Karimi & Akylas (2014) considered an expansion with not only the underlying wave beam but also the superimposed subharmonic wave packets that appear to order μ . The derivation of the wave interaction equations leads to six coupled equations for the two primary beam envelopes (two because of the two phases) and the four (two times two) subharmonic wave packet envelopes. Fortunately, this system can be reduced at leading order to only three coupled equations with three unknowns.

Taking a distinguished limit in which not only the amplitude of the primary wave, but also the nonlinear, dispersive, and viscous terms are small, Karimi & Akylas (2014) obtained a reduced description of the dynamics. The strategy is, as usual, to choose the scaling in order to get comparable magnitudes of the different terms. Interestingly, as only the quadratic interaction is potentially destabilizing for the primary beam, they compared it with the advection term for subharmonic waves: Because the former is smaller, this confirms that the resonant interaction cannot feed the instability in the limited time during which perturbations are in contact with the underlying beam. Beams with a general profile of finite width are thus stable to TRI.

Next, Karimi & Akylas (2014) considered the case of beams with profiles in the form of a monochromatic carrier with $\mathcal{O}(1)$ wavelength, modulated by a confined envelope. The complex envelopes of the primary wave $\psi_0(\eta, \tau)$ and of the secondary wave $\psi_{\pm}(\eta, \tau)$, which are functions of the cross-beam direction η (see **Figure 1**) and of the appropriate slow time τ , are thus generalizations of the plane wave solutions considered in Section 3.2.1. We recover these solutions with an envelope function independent of the cross-beam coordinate η , whereas an internal wave beam (such as the one in **Figure 3**) will correspond to $\Psi_0(\eta) = 1/2$ for $|\eta| < 1/2$, and $\Psi_0(\eta) = 0$ otherwise. With the introduction of the appropriate change of variables and rescaling of the relevant variables, the beam envelope Ψ_0 and the complex subharmonic envelopes Ψ_{\pm} are linked through



the following three coupled dimensionless equations:

$$\frac{\partial \Psi_{\pm}}{\partial \tau} = -\mathbf{c}_{g,\pm} \cdot \mathbf{e}_{k_0} \frac{\partial \Psi_{\pm}}{\partial \eta} - \bar{\nu} \kappa^2 \Psi_{\pm} + i \frac{N \kappa^2}{\omega_0} \sin^2 \chi |\Psi_0|^2 \Psi_{\pm} + \varpi \Psi_0 \Psi_{\mp}^*, \quad 19.$$

$$\frac{\partial \Psi_0}{\partial \tau} = -2\varpi \Psi_+ \Psi_-, \quad 20.$$

where $\bar{\nu}$ is the renormalized viscous dissipation, $\kappa = 2/\mu$ is a rescaled wave number modulus, $\chi = \theta - \phi$ and $\varpi = \sin \chi \cos^2(\chi/2)$ are two geometrical parameters, τ is the appropriate slow time for the evolution of the subharmonic wave packets, and η is the appropriate cross-beam coordinate.

In the appropriate distinguished limit identified by Karimi & Akylas (2014), the nonlinear term is balanced by the viscous term as in Section 3.4, but also by the transport term. The coupling between the evolution equations occurs through the nonlinear terms, which allow energy exchange between the underlying beam and subharmonic perturbations. The subsequent behavior of the complex envelopes Ψ_{\pm} determines the stability of the beam: If they are able to extract energy via nonlinear interaction with Ψ_0 at a rate exceeding the speed of linear transport and viscous decay, the beam is unstable.

From this system, it is in principle possible to study the stability of any profile. For example, a time-independent beam [$\Psi_0(\eta)$, $\Psi_{\pm} = 0$] is a steady-state solution of this system of three equations. The study of its stability relies on looking for the normal mode solutions $\Psi_{\pm} \propto \exp(\sigma \tau)$. For a plane wave, one obtains the growth rate $\sigma = [\sin \chi \cos^2(\chi/2)]/2 - \bar{\nu} \kappa^2$. A subtle point was carefully emphasized by Karimi & Akylas (2014). The above expression for σ seems independent of the wave vector disturbance κ in the inviscid limit, but the derivation has extensively used the hypothesis of fine-scale disturbances, which will of course break down for $\kappa \ll 1$. The maximum growth rate is indeed attained for finite but small κ . Uniform beams (internal plane waves with a confined envelope) are unstable if the beam is wide enough.

Karimi & Akylas (2014) also provided the solution to the initial value problem for a beam with $\Psi_0(\eta)$ tending toward zero as η tends to infinity. They showed the existence of a minimum value for the unstable perturbation wave number $\kappa_{\min} = \pi c_{g,\pm} / [2\varpi W \int_{-\infty}^{+\infty} \Psi_0(\eta) d\eta]$, corresponding to a maximum wavelength. Therefore, the possible spatial scale window for secondary wavelengths shrinks toward smaller scales as the beam is made narrower. Outside this range, no instability is possible even in the inviscid case.

Karimi & Akylas (2014) also analytically derived the minimum width explicitly for the top hat profile used in the experiments by Bourget et al. (2013) [$\Psi_0(\eta) = 1/2$ for $|\eta| < 1/2$ and $\Psi_0(\eta) = 0$ otherwise, as shown in **Figure 3**]. They argued that the existence of a minimum width is valid for a general profile. This minimum is dependent on the beam shape.

To summarize, internal plane waves with a confined envelope are unstable if the beam is wide enough, whereas weakly nonlinear beams with a general but confined profile (i.e., without any dominant carrier wave number) are stable with respect to short-scale subharmonic waves.

3.6. Effect of a Mean Advective Flow

G. Lerisson & J.M. Chomaz (unpublished manuscript; see also Lerisson 2017) have recently theoretically and numerically studied the TRI of an internal gravity beam in the presence of a mean advective flow. They keep the local wave vector and wave frequency constant in the frame moving with the fluid in order to encompass both tidal flows and lee waves.

Their main result is that, by impacting the group velocity of the primary and secondary waves, the mean advection velocity modifies the most unstable triads. They have predicted and



numerically confirmed that a strong enough advective flow enhances the instability of the central branch (leading to large-scale mode because one secondary wavelength is larger than the primary one) with respect to the external branch. However, the model is not able to explain the existence of an interesting stable region at intermediate velocity in their numerical simulations. To explain this, one must take into account the spatial growth of the secondary waves within the internal wave beam. A theory relying on the extension of the classical absolute or convective instability has not yet been derived.

3.7. Effect of the Rotation

Stratified fluids in geophysical situations generally also involve the effect of Earth’s rotation, modifying the properties of internal waves, as we discuss in this section.

3.7.1. Theoretical study. When one includes Coriolis effects due to Earth’s rotation at a rate Ω_C , the dispersion relation of internal waves is modified, and this of course has consequences for the group velocity, which we showed to be intimately related to the stability of internal wave beams. Bordes et al. (2012a) have reported experimental signatures of TRI of inertial gravity beams in a homogenous rotating fluid. It is thus expected that TRI will also show up when considering stratified rotating fluids.

Assuming invariance in the transverse y direction, the flow field may be written as $(u_x, u_y, u_z) = (\partial_z \psi, u_y, -\partial_x \psi)$, where $\psi(x, z, t)$ is the stream function of the nondivergent flow in the vertical plane and $u_y(x, z, t)$ is the transverse velocity. With the introduction of the Coriolis parameter $f = 2\Omega_C \sin \beta$, where β is the latitude, the dynamics of the flow field is given by the following system of three equations:

$$\partial_t b + J(b, \psi) - N^2 \partial_x \psi = 0, \tag{21}$$

$$\partial_t \nabla^2 \psi + J(\nabla^2 \psi, \psi) - f \partial_z u_y = -\partial_x b + \nu \nabla^4 \psi, \tag{22}$$

$$\partial_t u_y + J(u_y, \psi) + f \partial_z \psi = \nu \nabla^2 u_y, \tag{23}$$

in which the equation for the buoyancy perturbation is not modified, whereas Equation 4 has been modified and is now coupled to the dynamics of the transverse velocity u_y .

As previously noted, one can study beams of general spatial profiles, corresponding to the superposition of time-harmonic plane waves with the dispersion relation in Equation 8 modified to $\omega^2 = N^2 \sin^2 \theta + f^2 \cos^2 \theta$. The next step is again to look for subharmonic perturbations in the form of fine-scale (with respect to the width of the beam), nearly monochromatic wave packets with frequencies close to half of the primary frequency. It is straightforward to see that subharmonic waves propagate with an inclination ϕ given by $\sin \phi = [(\omega_0^2/4 - f^2)/(N^2 - f^2)]^{1/2}$ that vanishes when $\omega_0/2 = f$, i.e., at the critical latitude $\beta \approx 28.8^\circ$ (MacKinnon & Winters 2005). The modulus of the group velocity of subharmonic waves $c_{g,\pm} = (N^2 - f^2) \sin(2\phi)/(\omega_0 k_\pm)$ will thus also vanish at this latitude. The rotation dramatically reducing the ability of subharmonic waves to escape may seriously reinforce the instability.

Karimi & Akylas (2017) have shown that it is possible to reproduce the asymptotic analysis of the TRI with the inclusion of Earth’s rotation (see also Karimi 2015). One ends up with an unchanged Equation 20 for the dynamics of the primary wave, whereas the coupled dynamics of subharmonic waves is modified as follows:

$$\frac{\partial \Psi_\pm}{\partial \tau} = -\mathbf{c}_{g,\pm} \cdot \mathbf{e}_{k_0} \frac{\partial \Psi_\pm}{\partial \eta} + \frac{i}{2} \frac{3f}{\kappa^2 N} \frac{\partial^2 \Psi_\pm}{\partial \eta^2} - \bar{\nu} \kappa^2 \Psi_\pm + i \delta \kappa^2 \left| \frac{\partial \Psi_0}{\partial \eta} \right|^2 \Psi_\pm - \gamma \frac{\partial^2 \Psi_0}{\partial \eta^2} \Psi_\pm^*, \tag{24}$$



where the parameters δ and γ depend on the Coriolis parameter f and vanish when f tends to zero. The important modification is the second linear term on the right-hand side due to dispersion. It is important here because the first one may disappear given that the projection of the respective group velocity $\mathbf{c}_{g,\pm}$ of subharmonic envelopes Ψ_{\pm} on the cross-beam direction \mathbf{e}_{k_0} may vanish.

Karimi & Akylas (2017) first considered weakly nonlinear sinusoidal wave trains, emphasizing two interesting limits. On the one hand, the case far from the critical latitude allows one to recover the results of Section 3.5, in which there is no preferred wavelength of instability in the inviscid limit. On the other hand, when the group velocity of perturbations vanishes at the critical latitude, energy transport is due solely to second-order dispersion. This process of energy transport leads to the selection of a preferred wave number, independent of damping effects, which may suppress the instability for a sufficiently large damping factor, permitting the underlying wave to survive the instability. Karimi & Akylas (2017) obtained an expression for the growth rate identical to the result in the inviscid limit of Young et al. (2008) that explains that, at the critical latitude, additional physical factors, such as scale-selective dissipation, must become important. Hazewinkel & Winters (2011) have shown this result numerically, in agreement with in situ measurements (Alford et al. 2007).

For beams, there is always competition between energy extraction from the beam, which varies with beam profile, and the proximity to the critical latitude, without forgetting the viscous effects on the fine-scale structure of disturbances. Through numerical computations, it is possible to predict the stability properties for a given profile. In general, it turns out that rotation plays a significant role in dictating energy transfer from an internal wave to fine-scale disturbances via TRI under resonant configurations.

3.7.2. Experimental study. Maurer et al. (2016) were the first to conduct a laboratory experiment that studied the influence of rotation on the triadic instability of inertia gravity waves in a rotating stratified fluid. In this study, the setup used by Bourget et al. (2013, 2014) was placed on a rotating platform with a range of rotation rates from 0 to 2.16 rpm, allowing the dimensionless Coriolis parameter f/N to vary from 0 to 0.45.

One of their main observations was that the TRI threshold frequency is lowered by about 20% compared to the nonrotating case. An extension of the energy approach developed in Section 3.4 to the rotating case confirms this observation by showing that the finite-width effect of the beam width is reduced when rotation increases. This enhancement of TRI only applies to a limited range of rotation rates because when the rotation rate exceeds half of the primary wave frequency, the dispersion relation does not allow the lowest-frequency secondary wave, thereby inhibiting TRI. The competition between this limit and the finite-width effect reduction by rotation results in a minimum value for the frequency threshold. The position of this minimum, observed around $f/\omega_0 \approx 0.35$ in the experiment, depends on the Reynolds number, defined as $Re = \Psi_0/\nu$. The transposition of this result to high-Reynolds number situations like the ocean shows that the TRI enhancement is then localized in a narrow Coriolis parameter range, with $f = \omega_0/2$, thus recovering the critical latitude phenomenon.

When global rotation is applied to the fluid, another interesting feature is that it creates an amplitude threshold for TRI. Indeed, as discussed in Section 3.2.3, plane waves are always unstable in the absence of rotation. However, as shown in this section, the instability at very low amplitude occurs when \mathbf{k}_+ tends toward \mathbf{k}_0 , implying $\omega_+ \rightarrow \omega_0$ and therefore $\omega_- \rightarrow 0$. However, when there is rotation in the system, a zero-frequency subharmonic wave is blocked, hence the appearance of an amplitude threshold, which increases with f/N .



4. STREAMING INSTABILITY

4.1. Introduction

Another important mechanism for the instability of internal gravity waves beams is the generation of a mean flow, which Kataoka & Akylas (2015) called streaming instability (not to be confused with the mechanism for planetesimal formation in astrophysics). Andrews & McIntyre (1978) and Lighthill (1978b) noticed that internal gravity wave beams share several properties with acoustic wave beams. In particular, both kinds of waves may be subject to streaming in the presence of dissipative effects. Streaming refers here to the emergence of a slowly evolving, nonoscillating, Eulerian flow forced by nonlinear interactions of the oscillating wave beam with itself (Nyborg 1965, Lighthill 1978a). As reviewed by Riley (2001), it is now recognized that streaming actually occurs in a variety of flow models and remains an active field of research for both theoretical (Xie & Vanneste 2014) and experimental (Chraïbi et al. 2011, Squires & Quake 2013, Moudjed et al. 2014) points of view.

The fact that dissipative effects are required to irreversibly generate a mean flow through the nonlinear interactions of a wave beam with itself can be thought of as a direct consequence of nonacceleration arguments that came up 50 years ago in the geophysical fluid dynamics context, with important contributions from Charney & Drazin (1961), Eliassen & Palm (1961), and Andrews & McIntyre (1976), among others. Plumb (1977) used those ideas to propose an idealized model for the quasi-biennial oscillation (QBO), together with an experimental simulation of the phenomenon (Plumb & McEwan 1978). The oscillations require more than one wave beam, but Plumb (1977) discussed first how a single wave beam propagating in a vertical plane could generate a mean flow. He predicted the vertical shape of this mean flow, emphasizing the important role played by the wave attenuation through dissipative effects. The experiment by Plumb & McEwan (1978) may be thought of as the first quantitative observation of streaming in stratified fluids.

Those examples correspond, however, to a very peculiar instance of streaming, with no production of vertical vorticity. By contrast, most applications of acoustic streaming since the earlier works of Eckart (1948) and Westervelt (1953) involve the production of vorticity by an irrotational wave. As far as vortical flows are concerned, Lighthill (1978b) noticed important analogies between acoustic waves and internal gravity waves: In both cases, vortical flows and propagating waves are decoupled at a linear level in the inviscid limit, and steady streaming results from viscous attenuation of the wave amplitude. In particular, Lighthill (1978b) noticed that streaming could generate a flow with vertical vorticity. However, experimental observation of the emergence of a vortical flow in stratified fluids through this mechanism remained elusive until recently. While studying the internal wave generation process via a tidal flow over 3D seamounts in a stratified fluid, King et al. (2009) observed a strong flow in the plane perpendicular to the oscillating tidal flow. For low forcing, this flow was found to be proportional to the square of the forcing amplitude. That led them to invoke nonlinear interactions, either between the internal wave beam and itself, or between internal waves and the viscous boundary layer. The analysis was not pursued further, and the sign of the vorticity generated, opposite to the one discussed in the following subsections, remains puzzling.

A few years later, studying the reflection of an internal wave beam on a sloping bottom, Grisouard and his collaborators have also discovered this mean flow generation in experiments (Grisouard 2010, Leclair et al. 2011, Grisouard et al. 2013). The basic configuration was a uniform beam reflecting onto a simple slope in a uniformly stratified fluid. As predicted (Dauxois & Young 1999, Gostiaux et al. 2006), the interaction between the incident and reflected waves produced harmonic waves, thereby reducing the amplitude of the reflected wave. However, more



surprisingly, they found that the reflected wave was nearly absent because a wave-induced mean flow appeared in the superposition region of the incident and reflected waves, progressively growing in amplitude. Comparing 2D and 3D numerical simulations, they showed that this mean flow is of dissipative origin and 3D. [However, transient mean flows can be generated by inviscid motion in the wake of a propagating internal wave packet (Bretherton 1969, van den Bremer & Sutherland 2014).] Its presence totally modifies the 2D view considered in the literature for reflection of internal waves. Indeed, there have been many interesting theoretical studies of internal gravity wave–mean flow interactions (Bretherton 1969, Lelong & Riley 1991, Tabaei & Akylas 2003), but none of them considered the effect of dissipation in three dimensions.

The complete and theoretical understanding of the generation of a slowly evolving vortical flow by an internal gravity wave beam was possible using an even simpler setup. Bordes et al. (2012b) reported observations of a strong mean flow accompanying a time-harmonic internal gravity beam freely propagating in a tank significantly wider than the beam. Below we describe in detail the experimental setup and the observations, together with two related theories by Bordes et al. (2012b) and Kataoka & Akylas (2015), which account for the spatial structure and temporal evolution of the mean flow and illuminate the mechanism of instability. Those approaches bear strong similarities with the result of Grisouard & Bühler (2012), who used generalized Lagrangian mean theory in order to describe the emergence of a vortical flow in the presence of a barotropic tide’s oscillating flow above topography variations.

4.2. Experimental Observations

Bordes et al. (2012b) have studied an internal gravity wave beam of limited lateral extent propagating along a significantly wider stratified fluid tank. Previously, most experimental studies using the same internal wave generator (Gostiaux et al. 2007, Mercier et al. 2010) were quasi-2D (beam and tank of equal width) and therefore were without significant transversal variations.

Figure 4a presents a schematic view of the experimental setup in which one can see the generator, the tank, and the representation of the internal wave beam generated (see Bordes 2012 for additional details). The direct inspection of the flow field shows an unexpected and

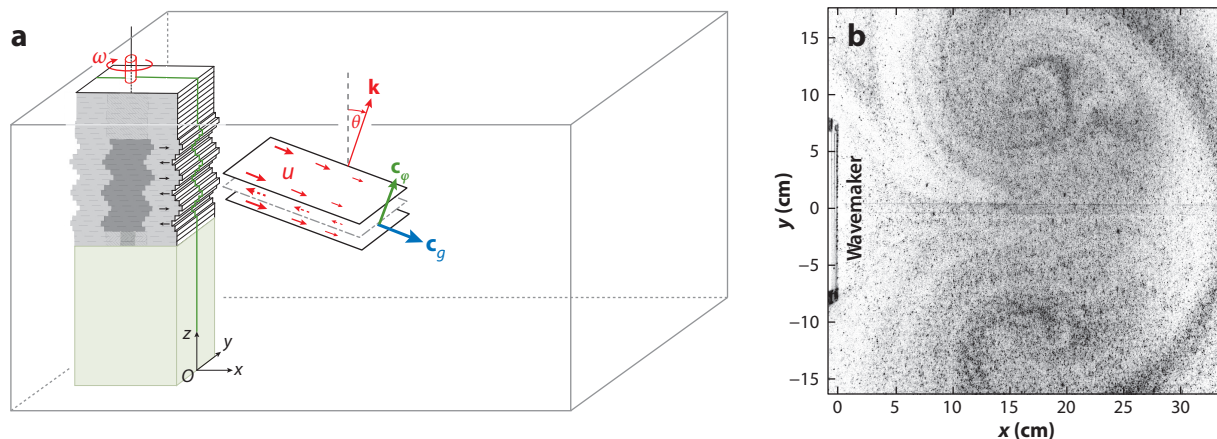


Figure 4 (a) Schematic representation of the experimental setup (Bordes et al. 2012b) with the generator on the left of the tank. (b) Top view of the particle flow in a horizontal plane at intermediate depth.

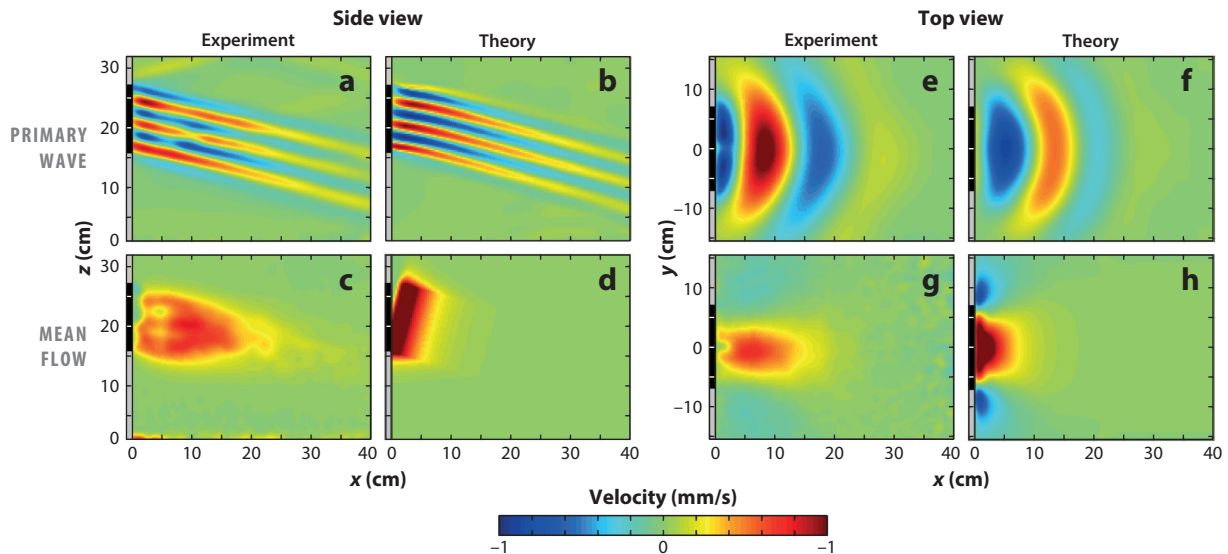


Figure 5

(*Top row*) Experimental and theoretical horizontal velocity fields u_x for the primary wave (Bordes et al. 2012b), obtained by filtering (Mercier et al. 2008) the velocity field at the forcing frequency. (*Bottom row*) Experimental and theoretical horizontal velocity fields u_x for the mean flow (Kataoka & Akylas 2015), obtained by low-pass filtering the velocity field. Panels *a–d* present side views, whereas panels *e–h* show top views. The wave generator (along the black line on the left side of each plot) is represented in gray with its moving part in black.

spontaneously generated pair of vortices, emphasized in **Figure 4b** by the tracer particles dispersed in the tank to visualize the flow field using particle image velocimetry. This structure is actually a consequence of the generation of a strong mean flow. This experiment therefore provides an excellent setup for carefully studying the mean flow generation and providing a theoretical understanding that explains the salient features of the experimental observations.

These observations are summarized in **Figure 5**, which shows side and top views not only of the generated internal wave beam, but also of its associated mean flow. One sees that the wave part of the flow is monochromatic, propagating at an angle θ and with an amplitude varying slowly in space compared to the wavelength λ . These waves are accompanied by a mean flow with a jet-like structure in the direction of the horizontal propagation of waves, together with a weak recirculation outside the wave beam. Initially produced inside the wave beam, this dipolar structure corresponds to the spontaneously generated vortex shown in **Figure 4b**. Moreover, the feedback of the mean flow on the wave leads to a transverse bending of wave beam crests apparent in **Figure 5e,f**.

4.3. Analytical Descriptions

Let us now consider several analytical approaches that have been successively used to tackle the issue of streaming instability.

4.3.1. A preliminary multiple scale analysis. Taking advantage of the physical insights provided by the experiments, Bordes et al. (2012b) have proposed an approximate description that uses a time-harmonic wave flow with a slowly varying amplitude in space. The problem contains two

key nondimensional numbers, the Froude number $U/\lambda N$ and the ratio $\nu/\lambda^2 N$ between the wavelength λ and the attenuation length scale of the wave beam due to viscosity, $\lambda^3 N/\nu$ (Mercier et al. 2008). For analytical convenience, they considered a distinguished limit with the small parameter $\varepsilon = Fr^{1/3}$, together with the scaling $\nu/\lambda^2 N = \varepsilon/\lambda_\nu$ where $\lambda_\nu \approx 1$. As usual, the appropriate scaling in the small parameter ε is deduced from a mix of physical intuition and analytical handling of the calculations. In their case, Bordes et al. (2012b) were looking for a regime with small nonlinearity and dissipation. In terms of the velocity components (u_x, u_y, u_z) , the buoyancy b , and the vertical vorticity $\Omega = \partial_x u_y - \partial_y u_x$, the governing dimensionless equations in this 3D setting read

$$\nabla_H \cdot \mathbf{u}_H = -\partial_z u_z, \tag{25}$$

$$\partial_t b + \varepsilon^3 (\mathbf{u} \cdot \nabla b) + u_z = 0, \tag{26}$$

$$\partial_t \Omega + \varepsilon^3 [\mathbf{u}_H \cdot \nabla_H \Omega + (\nabla_H \cdot \mathbf{u}_H) \Omega + \partial_x (u_z \partial_z u_y) - \partial_y (u_z \partial_z u_x)] = \varepsilon \lambda_\nu^{-1} \nabla^2 \Omega, \tag{27}$$

$$\begin{aligned} \nabla^2 \partial_t u_z + \nabla_H^2 u_z &= \varepsilon \lambda_\nu^{-1} \nabla^4 \partial_t u_z \\ &\quad - \varepsilon^3 \left\{ \partial_t [\nabla_H^2 (\mathbf{u} \cdot \nabla u_z) - \partial_z \nabla_H (\mathbf{u} \cdot \nabla \mathbf{u}_H)] + \nabla_H^2 (\mathbf{u} \cdot \nabla b) \right\}, \end{aligned} \tag{28}$$

in which the index H in \mathbf{u}_H and ∇_H reduces to the horizontal velocity field, gradient, or Laplacian operator.

Having appropriately adimensionalized the equation via the introduction of the rescaled spatial and temporal coordinates, we are now in a good position to perform a multiple scale analysis. Looking for a flow field in a perturbation series $u_r = u_r^0 + \varepsilon u_r^1 + o(\varepsilon)$ for $r = x, y$, or z with a priori $u_y^0 = 0$, as suggested by the structure of the beam, together with the vertical vorticity field $\Omega = \varepsilon^2 \Omega_2 + \varepsilon^4 \Omega_4 + o(\varepsilon^4)$, one can give the structure of the beam to the first three orders through a tedious but straightforward application of the multiple-scale framework (with $x_i = \varepsilon^i x$ and $t_i = \varepsilon^i t$). The first order ε^0 provides the expressions for u_x^0 and u_z^0 , the second order ε^1 gives the expression for u_y^1 , and the third order ε^2 shows that u_z^0 does not depend on the slow timescale t_2 .

Nonlinear terms contribute a priori for the first time to order ε^3 , but interestingly, one again finds (see Section 2.3) that they vanish to this order. To order ε^4 , one obtains that the term independent of the slow time t_0 vanishes, and thus, nonlinear terms do not induce a mean flow to this order either. It is only to order ε^5 that nonlinear terms directly contribute to the mean flow generation. The governing equation of the vortical flow induced by the mean flow is then given in the original dimensional units by

$$\partial_t \overline{\Omega} = \frac{\partial_{xy} \mathcal{U}^2}{(2 \cos \theta)^2} + \nu \nabla^2 \overline{\Omega}, \tag{29}$$

where the overline symbol stands for the filtering over one period and $\mathcal{U}(x, y)$ is the amplitude of the wave envelope.

Several conclusions can be directly inferred from this analysis. First, as emphasized by the first term on the right-hand side of Equation 29, nonlinear terms are crucial as a source of vertical vorticity. Note that one recovers that the amplitude of the mean flow is proportional to the square of the wave amplitude, as has been found in experimental (King et al. 2009) or theoretical (Buhler 2009) results. Second, the variations of the wave field in the y direction (implying $\partial_y \neq 0$) are necessary for nonlinearities to be a source of vertical vorticity. This illuminates why 3D effects are crucial and therefore why no mean flow generation was noticed in two dimensions (Mercier et al. 2010, Grisouard et al. 2013). Finally, the viscous attenuation of the wave field in the x direction (implying $\partial_x \neq 0$) is also necessary to produce vertical vorticity. In actual experiments, variations



of the amplitude in the x direction can also come from finite-width effects but are not sufficient to generate a mean flow.

One drawback of the above approach, however, is that it does not describe the feedback of the mean flow on the waves. For this reason, the approach becomes inconsistent at long times in the far field region.

The above combined experimental and analytical proof of the key role played by the wave beam amplitude's viscous attenuation and lateral variation in the generation of the observed mean flow has therefore motivated a more careful asymptotic expansion by Kataoka & Akylas (2015), taking into account the two-way coupling between waves and mean flow. This two-way coupling accounts for the horizontal bending of the wave mean field in Bordes et al.'s (2012b) experiments, as explained in Section 4.3.3.

4.3.2. Stability to three-dimensional modulations. Initially, Kataoka & Akylas (2013) were interested in 3D perturbations of internal wave beams. Specifically, they studied the stability of uniform beams subject to oblique modulations that vary slowly in the along-beam ξ and the transverse-horizontal y directions (see **Figure 1**). The results turned out to be fundamentally different from that of purely longitudinal modulations considered in Tabaei & Akylas (2003). Due to transverse variations, a resonant interaction becomes possible between the primary beam and 3D perturbations. Moreover, their analysis revealed that 3D perturbations are accompanied by circulating horizontal mean flows far from the beam.

Kataoka & Akylas (2013) studied the linear stability of uniform internal wave beams with confined spatial profiles by introducing infinitesimal disturbances to the basic state in the form of normal modes, not only in the along-beam direction ξ but also in the transverse-horizontal direction y . They used an asymptotic approach, valid for long wavelength perturbations relative to the beam thickness. The boundary conditions, combined with the matching conditions between the solution near and far from the beam, ensure that the primary-harmonic and mean flow perturbations are confined in the cross-beam direction.

The analysis brings out the coupling of the primary-harmonic and mean flow perturbations to the underlying internal wave beam: The interaction of the primary-harmonic perturbation with the beam induces a mean flow, which in turn feeds back to the primary harmonic via interactions with the beam. Whether this primary-harmonic–mean flow interaction mechanism can extract energy from the basic beam, causing instability, depends upon finding modes that remain confined in the cross-beam direction.

4.3.3. Complete model for the three-dimensional propagation of small-amplitude internal wave beams. In a second stage, Kataoka & Akylas (2015) have derived a complete matched asymptotic analysis of the experiment performed by Bordes et al. (2012b) for a 3D, weakly nonlinear, and uniformly stratified viscous Boussinesq fluid. From their prior experience (Tabaei & Akylas 2003, Kataoka & Akylas 2013), Kataoka & Akylas (2015) have chosen the along-beam stretched spatial coordinate as $\Xi = \varepsilon^2 \xi$, the slow time as $T = \varepsilon^2 t$, and the transverse-horizontal variations as $Y = \varepsilon y$, so that along-beam and transverse dispersions are comparable, together with variations in the cross-beam direction η (see **Figure 1**). Combining this choice with a small nonlinearity scaling as $\varepsilon^{1/2}$ and a weak viscous dissipation $\bar{\nu}\varepsilon^2$ that carry equal weight, they were able to fully analyze the mean flow, separately near and far from the beam, before matching both solutions.

Kataoka & Akylas (2015) derived a closed system of two coupled equations linking the amplitude of the primary time harmonic \mathcal{U} and the mean flow component \bar{V}_∞ of the cross-beam velocity field. The latter appears to be necessary for matching with the mean flow far from the beam. The



equation governing the dynamics of the mean flow reads

$$\partial_T \bar{V}_\infty = \cos \theta \partial_Y \mathcal{H} \left[\int_{-\infty}^{+\infty} d\eta \mathcal{U}^* \left(\frac{\partial \mathcal{U}}{\partial \Xi} + \frac{\cot \theta}{2} \int^n d\eta \frac{\partial^2 \mathcal{U}}{\partial Y^2} \right) \right], \quad 30.$$

where $\mathcal{H}(\cdot)$ stands for the Hilbert transform in the transverse coordinate Y . This immediately shows that transverse variations ($\partial_Y \neq 0$) of the beam are essential for having a nonzero source term.

Because the generated mean vertical vorticity is given at leading order by $\bar{\Omega} = \cos \theta \partial_Y \bar{\mathcal{U}} = (\cos^2 \theta / \sin \theta) \partial_Y \bar{V}_\infty + \mathcal{O}(\varepsilon^{1/2})$, a direct comparison of these results with Equation 29 is possible. The first term in Equation 30, which involves derivatives in both horizontal coordinates, corresponds to the term identified by Bordes et al. (2012b), whereas this more complete analysis sheds light on an additional term deriving from purely transverse variations.

Using an intermediate equation, Kataoka & Akylas (2015) ended finally with the alternative and more elegant form

$$\partial_T \bar{V}_\infty = i \partial_Y \mathcal{H} \left[\int_{-\infty}^{+\infty} d\eta [(\mathcal{U}^* \partial_\eta \mathcal{U})_T + \bar{v} \partial_\eta \mathcal{U}^* \partial_\eta \mathcal{U}] \right]. \quad 31.$$

Moreover, they showed that to match inner and outer solutions, this induced mean flow turns out to be purely horizontal to leading order and also dominant over the other harmonics. The comparison of this theoretical description agrees very well with the experimental results, as beautifully illustrated in **Figure 5**.

As far as a comparison with the experimental results of Bordes et al. (2012b) is concerned, a common caveat of the predictions by Bordes et al. (2012b) and Kataoka & Akylas (2015) is the assumption of a small wavelength compared to the length scale of the wave envelope, which is only marginally satisfied in the experiments. For instance, one may wonder if the horizontal structure of the observed waves is primarily due to the feedback of the mean flow on the wave or to the sole diffraction pattern of the wave due to this absence of scale separation. This needs to be addressed in future works.

4.4. Forcing of Oceanic Mean Flows

Using an analysis based on generalized Lagrangian mean theory, Grisouard & Bühler (2012) have also studied the role of dissipating oceanic internal tides in forcing mean flows. For analytical convenience, they modeled wave dissipation as a linear damping term $-\gamma_b b$ in the buoyancy Equation 3 and neglected the viscous term in the momentum Equation 2.

Within this framework, Grisouard & Bühler (2012) discussed in detail the range of situations in which a strong, secularly growing mean flow response can be expected. Their principal results include the derivation of an expression for the effective mean force exerted by small-amplitude internal tides on oceanic mean flows. At leading order, taking into account the background rotation and using a perturbation series in small wave amplitude, they derived the following explicit expression:

$$\partial_t \bar{\Omega} + \frac{\gamma_b f}{N^2} \partial_z \bar{b} = \frac{-i \gamma_b N^2}{2(\omega^2 + \gamma_b^2) \omega} (\nabla u_z^* \times \nabla u_z) \cdot \mathbf{e}_z \quad 32.$$

for the average over the tidal period of the vertical vorticity. It is remarkable that in the presence of rotation one recovers a forcing term on the right-hand side that is analogous to those obtained by Bordes et al. (2012b) and Kataoka & Akylas (2015) in the nonrotating case. In inviscid rotating flows, vortical modes are at geostrophic equilibrium, and there is a frequency gap separating those geostrophic modes from inertia gravity waves. This frequency gap generally precludes interactions



between geostrophic modes and wave modes. However, Grisouard & Bühler (2012) showed that the combination of nonlinear and dissipative effects allows for a one-way energy transfer from inertia gravity wave modes to geostrophic modes through a genuinely 3D mechanism. Using Equation 32, Grisouard & Bühler (2012) computed the effective mean force numerically in a number of idealized examples with simple topographies.

Although a complete formulation with dissipative terms in the momentum equation is necessary, Grisouard & Bühler's (2012) conclusion is that energy of inertia gravity waves in rotating fluids can be transferred to a horizontal mean flow by a similar resonance mechanism, as described by Bordes et al. (2012b). One therefore understands that mean flows can be generated in regions of wave dissipation and not necessarily near the topographic wave source.

5. CONCLUSIONS AND FUTURE DIRECTIONS

Several recent experimental and theoretical works have renewed interest in internal wave beams, which are ubiquitous in stratified fluids because they are solutions of the nonlinear governing equations. This review has presented the two main mechanisms of instability for those beams: TRI and streaming instability, which we discuss in turn below.

First, we have shown that TRI produces a direct transfer of energy from large scales (primary waves) to smaller scales (subharmonic ones) for inviscid plane waves, but that this is not the case for internal wave beams because the most unstable triad may combine subharmonic waves with larger and smaller wavelengths. Moreover, the effects of the finite width and envelope shape on the onset of TRI have been overlooked. Researchers have to take these features into account in order to safely reproduce the complete nonlinear transfer of energy between scales in the ocean interior or in an experimental analog (Scolan et al. 2013, Brouzet et al. 2016a), and therefore to find its stationary state, the so-called Garrett–Munk Spectrum (Garrett & Munk 1975) or its possible theoretical analog, the Zakharov spectrum for the wave turbulence theory (Nazarenko 2011).

Second, now that the mechanism underlying the streaming instability and the conditions for its occurrence have been identified, several other examples will probably be reported in the coming years. For example, such mean flow generation has also been observed in a recent experiment (Brouzet et al. 2016b) for which the reflection of internal gravity waves in closed domains leads to an internal wave attractor. Two lateral Stokes boundary layers generate a fully 3D interior velocity field that provides the condition for the mean flow to appear. With a perturbation approach, Beckebanze & Maas (2016) confirmed this theoretically and showed that the generated 3D velocity field damps the wave beam at high wave numbers, thereby providing a new mechanism for establishing an energetic balance for steady-state wave attractors. Recently, Semin et al. (2016) have also experimentally studied the generation of a mean flow by a progressive internal gravity wave in a simple 2D geometry, revisiting an experimental analog of the QBO (Plumb & McEwan 1978). Semin et al. (2016) studied the feedback of the mean flow on the wave, an essential ingredient of the QBO.

Which is the dominant mechanism? Kataoka & Akylas (2016) have recently suggested that streaming instabilities are central to 3D internal gravity wave beam dynamics, in contrast to the TRIs of sinusoidal wave trains relevant to uniform beams, the special case of an internal plane wave with a confined spatial profile. This review therefore reinforces the need for more 3D experiments studying wave-induced mean flow. In particular, what are the factors that favor mean flow generation with respect to triadic interaction? Are they angles of propagation, three-dimensionality, or stratification? These are important questions that need to be addressed.



SUMMARY POINTS

In an incompressible, nonrotating, and linearly stratified Boussinesq fluid, the following conclusions can be drawn:

1. Plane waves are solutions of the linear and nonlinear equations for any amplitude.
2. Internal wave beams, which correspond to the superposition of plane waves with wave vectors of different magnitudes but pointing in the same direction, are solutions to the linear and nonlinear equations.
3. Plane wave solutions are always unstable by TRI.
4. General localized internal wave beams are stable, whereas (quasi) spatial-harmonic internal wave beams are unstable if the beams are wide enough.
5. In the presence of rotation, beams of general spatial profiles are more vulnerable to TRI especially close to the critical latitude where nearly stationary wave packets remain in the interaction region for extended durations, facilitating energy transfer.
6. Internal gravity wave beams with confined spatial profiles are linearly unstable to 3D modulations.
7. When a wave beam is attenuated along its direction of propagation and when the wave envelope varies in the transverse-horizontal direction, nonlinear interactions of the wave beam with itself induce the emergence of a horizontal mean flow with vertical vorticity.

DISCLOSURE STATEMENT

The authors are not aware of any biases that might be perceived as affecting the objectivity of this review.

ACKNOWLEDGMENTS

This work was supported by the LABEX iMUST grant ANR-10-LABX-0064 from the Université de Lyon, within the program Investissements d'Avenir, grant ANR-11-IDEX-0007, operated by the French National Research Agency (ANR). This work was accomplished thanks to the resources of the Pôle Scientifique de Modélisation Numérique (PSMN) from École Normale Supérieure de Lyon. We acknowledge the contributions to our research on this topic from G. Bordes, B. Bourget, C. Brouzet, P.-P. Cortet, E. Ermanyuk, M. Le Bars, P. Maurer, F. Moisy, J. Munroe, H. Scolan, and A. Wienkers. We thank T. Akylas, V. Botton, N. Grisouard, H. Karimi, T. Kataoka, L. Maas, T. Peacock, C. Staquet, and B. Voisin for helpful discussions.

LITERATURE CITED

- Alexander M. 2003. Parametrization of Physical process: gravity wave fluxes. In *Encyclopedia of the Atmospheric Sciences*, ed. J Holton, J Curry, J Pyle, pp. 1669–705. London: Academic
- Alford M, MacKinnon JA, Zhao Z, Pinkel R, Klymak J, Peacock T. 2007. Internal waves across the Pacific. *Geophys. Res. Lett.* 34:L24601
- Alford M, Peacock T, MacKinnon JA, Nash JD, Buijsman MC, et al. 2015. The formation and fate of internal waves in the South China Sea. *Nature* 521:65–69



- Andrews DG, McIntyre ME. 1976. Planetary waves in horizontal and vertical shear: the generalized Eliassen-Palm relation and the mean zonal acceleration. *J. Atmos. Sci.* 33:2031–48
- Andrews DG, McIntyre ME. 1978. An exact theory of nonlinear waves on a Lagrangian-mean flow. *J. Fluid Mech.* 89:609–46
- Beckebanze F, Maas LRM. 2016. Damping of 3D internal wave attractors by lateral walls. *Proc. Int. Symp. Strat. Flows, 8th., 29 Aug.–1 Sept.* San Diego: Univ. Calif. San Diego
- Bell TH. 1975. Lee waves in stratified flows with simple harmonic time dependence. *J. Fluid Mech.* 67:705–22
- Benielli D, Sommeria J. 1998. Excitation and breaking of internal gravity waves by parametric instability. *J. Fluid Mech.* 374:117–44
- Bordes G. 2012. *Interactions non-linéaires d'ondes et tourbillons en milieu stratifié ou tournant.* PhD Thesis, ENS Lyon. <https://tel.archives-ouvertes.fr/tel-00733175/en>
- Bordes G, Moisy F, Dauxois T, Cortet PP. 2012a. Experimental evidence of a triadic resonance of plane inertial waves in a rotating fluid. *Phys. Fluids* 24:014105
- Bordes G, Venaille A, Joubaud S, Odier P, Dauxois T. 2012b. Experimental observation of a strong mean flow induced by internal gravity waves. *Phys. Fluids* 24:086602
- Bourget B. 2014. *Ondes internes, de l'instabilité au mélange. Approche expérimentale.* PhD Thesis, ENS Lyon. <https://tel.archives-ouvertes.fr/tel-01073663/en>
- Bourget B, Dauxois T, Joubaud S, Odier P. 2013. Experimental study of parametric subharmonic instability for internal plane waves. *J. Fluid Mech.* 723:1–20
- Bourget B, Scolan H, Dauxois T, Le Bars M, Odier P, Joubaud S. 2014. Finite-size effects in parametric subharmonic instability. *J. Fluid Mech.* 759:739–50
- Bretherton FP. 1969. On the mean motion induced by internal gravity waves. *J. Fluid Mech.* 36:785–803
- Brouzet C, Ermanyuk EV, Joubaud S, Sibgatullin IN, Dauxois T. 2016a. Energy cascade in internal-wave attractors. *Europhys. Lett.* 113:44001
- Brouzet C, Sibgatullin IN, Scolan H, Ermanyuk EV, Dauxois T. 2016b. Internal wave attractors examined using laboratory experiments and 3D numerical simulations. *J. Fluid Mech.* 793:109–31
- Buhler OK. 2009. *Waves and Mean Flows.* Cambridge, UK: Cambridge Univ. Press
- Callies J, Ferrari R, Bühler O. 2014. Transition from geostrophic turbulence to inertia-gravity waves in the atmospheric energy spectrum. *PNAS* 111:17033–38
- Chalamalla VK, Sarkar S. 2016. PSI in the case of internal wave beam reflection at a uniform slope. *J. Fluid Mech.* 789:347–67
- Charney JG, Drazin PG. 1961. Propagation of planetary-scale disturbances from the lower into the upper atmosphere. *J. Geophys. Res.* 66:83–109
- Chraïbi H, Wunenburger R, Lasseux D, Petit J, Delville JP. 2011. Eddies and interface deformations induced by optical streaming. *J. Fluid Mech.* 688:195–218
- Clark HA, Sutherland BR. 2010. Generation, propagation, and breaking of an internal wave beam. *Phys. Fluids* 22:076601
- Cole ST, Rudnick DL, Hodges BA, Martin JP. 2009. Observations of tidal internal wave beams at Kauai Channel, Hawaii. *J. Phys. Oceanogr.* 39:421–36
- Craik AD. 1988. *Wave Interactions and Fluid Flows.* Cambridge, UK: Cambridge Univ. Press
- Dauxois T, Young WR. 1999. Near critical reflection of internal waves. *J. Fluid Mech.* 390:271–95
- Davis RE, Acrivos A. 1967. The stability of oscillatory internal waves. *J. Fluid Mech.* 30:723–36
- Eckart C. 1948. Vortices and streams caused by sound waves. *Phys. Rev.* 73:68–76
- Eliassen A, Palm E. 1961. On the transfer of energy in stationary mountain waves. *Geophys. Publ.* 22:1–23
- Fritts DC, Alexander MJ. 2003. Gravity wave dynamics and effects in the middle atmosphere. *Rev. Geophys.* 41:1003
- Garrett C, Kunze E. 2007. Internal tide generation in deep ocean *Annu. Rev. Fluid Mech.* 39:57–87
- Garrett C, Munk W. 1975. Space-time scales of internal waves: a progress report. *J. Geophys. Res.* 80:291–97
- Gayen B, Sarkar S. 2013. Degradation of an internal wave beam by parametric subharmonic instability in an upper ocean pycnocline. *J. Geophys. Res. Oceans* 118:4689–98
- Gerkema T, Staquet C, Bouruet-Aubertot P. 2006. Decay of semi-diurnal internal-tide beams due to subharmonic resonance. *Geophys. Res. Lett.* 33:L08604



- Gill AE. 1982. *Atmosphere–Ocean Dynamics*. New York: Academic
- Gostiaux L, Dauxois T. 2007. Laboratory experiments on the generation of internal tidal beams over steep slopes. *Phys. Fluids* 19:028102
- Gostiaux L, Dauxois T, Didelle H, Sommeria J, Viboud S. 2006. Quantitative laboratory observations of internal wave reflection on ascending slopes. *Phys. Fluids* 18:056602
- Gostiaux L, Didelle H, Mercier S, Dauxois T. 2007. A novel internal waves generator. *Exp. Fluids* 42:123–30
- Grisouard N. 2010. *Réflexions et réfractions non-linéaires d'ondes de gravité internes*. PhD Thesis, Univ. Grenoble. <http://tel.archives-ouvertes.fr/tel-00540608/en/>
- Grisouard N, Bühler O. 2012. Forcing of oceanic mean flows by dissipating internal tides. *J. Fluid Mech.* 708:250–78
- Grisouard N, Leclair M, Gostiaux L, Staquet C. 2013. Large scale energy transfer from an internal gravity wave reflecting on a simple slope. *Proc. IUTAM* 8:119–28
- Hasselmann K. 1967. A criterion for nonlinear wave instability. *J. Fluid Mech.* 30:737–39
- Hazewinkel J, Winters KB. 2011. PSI on the internal tide on a β plane: flux divergence and near-inertial wave propagation. *J. Phys. Oceanogr.* 41:1673–82
- Hibiya T, Nagasawa M, Niwa Y. 2002. Nonlinear energy transfer within the oceanic internal wave spectrum at mid and high latitudes. *J. Geophys. Res.* 107:3207
- Johnston TMS, Merrifield MA, Holloway PE. 2003. Internal tide scattering at the Line Islands Ridge. *J. Geophys. Res.* 108:3365
- Johnston TMS, Rudnick DL, Carter GS, Todd RE, Cole ST. 2011. Internal tidal beams and mixing near Monterey Bay. *J. Geophys. Res.* 116:C03017
- Joubaud S, Munroe J, Odier P, Dauxois T. 2012. Experimental parametric subharmonic instability in stratified fluids. *Phys. Fluids* 24:041703
- Karimi HH. 2015. *Parametric subharmonic instability of internal gravity wave beams*. PhD Thesis, Mass. Inst. Technol.
- Karimi HH, Akylas TR. 2014. Parametric subharmonic instability of internal waves: locally confined beams versus monochromatic wave trains. *J. Fluid Mech.* 757:381–402
- Karimi HH, Akylas TR. 2017. Near-inertial parametric subharmonic instability of internal gravity wave beams. *Phys. Rev. Fluids* 2:074801
- Kataoka T, Akylas TR. 2013. Stability of internal gravity wave beams to three-dimensional modulations. *J. Fluid Mech.* 736:67–90
- Kataoka T, Akylas TR. 2015. On three-dimensional internal gravity wave beams and induced large-scale mean flows. *J. Fluid Mech.* 769:621–34
- Kataoka T, Akylas TR. 2016. Three-dimensional instability of internal gravity beams. *Proc. Int. Symp. Strat. Flows, 8th, 29 Aug.–1 Sept.* San Diego: Univ. Calif. San Diego
- Khatiwalwa S. 2003. Generation of internal tides in an ocean of finite depth: analytical and numerical calculations. *Deep Sea Res. Part I* 50:3–21
- King B, Zhang HP, Swinney HL. 2009. Tidal flow over three-dimensional topography in a stratified fluid. *Phys. Fluids* 21:116601
- Koudella CR, Staquet C. 2006. Instability mechanisms of a two-dimensional progressive internal gravity wave. *J. Fluid Mech.* 548:165–96
- Lamb KG. 2004. Nonlinear interaction among internal wave beams generated by tidal flow over supercritical topography. *Geophys. Res. Lett.* 31:L09313
- Leclair M, Grisouard N, Gostiaux L, Staquet C, Auclair F. 2011. Reflexion of a plane wave onto a slope and wave-induced mean flow. *Proc. Int. Symp. Strat. Flows, 7th, 22–26 Aug.* Rome: Sapienza Univ. Roma
- Lelong M-P, Riley J. 1991. Internal wave-vortical mode interactions in strongly stratified flows. *J. Fluid Mech.* 232:1–19
- Lerisson G. 2017. *Étude de la stabilité globale et locale d'une onde de gravité interne en milieu linéairement stratifié*. PhD Thesis, École Polytech.
- Lerisson G, Chomaz JM. 2017. Global stability of internal gravity wave. *Phys. Rev. Fluids*
- Liang Y, Zareei A, Alam MR. 2017. Inherently unstable internal gravity waves due to resonant harmonic generation. *J. Fluid Mech.* 811:400–20



- Lien R-C, Gregg MC. 2001. Observations of turbulence in a tidal beam and across a coastal ridge. *J. Geophys. Res.* 106:4575–91
- Lighthill J. 1978a. Acoustic streaming. *J. Sound Vib.* 61:391–418
- Lighthill J. 1978b. *Waves in Fluids*. Cambridge, UK: Cambridge Univ. Press
- Lighthill J. 1996. Internal waves and related initial-value problems. *Dyn. Atmos. Oceans* 23:3–17
- MacKinnon JA, Alford MH, Sun O, Pinkel R, Zhao Z, Klymak J. 2013. Parametric subharmonic instability of the internal tide at 29°N. *J. Phys. Oceanogr.* 43:17–28
- MacKinnon JA, Winters KB. 2005. Subtropical catastrophe: significant loss of low-mode tidal energy at 28.9°. *Geophys. Res. Lett.* 32:L15605
- Maugé R, Gerkema T. 2008. Generation of weakly nonlinear nonhydrostatic internal tides over large topography: a multi-modal approach. *Nonlinear Process. Geophys.* 15:233–44
- Maurer P, Joubaud S, Odier P. 2016. Generation and stability of inertia-gravity waves. *J. Fluid Mech* 808:539–61
- McEwan AD. 1971. Degeneration of resonantly-excited standing internal gravity waves. *J. Fluid Mech.* 50:431–48
- McEwan AD. 1973. Interactions between internal gravity wave and their traumatic effect on a continuous stratification. *Bound.-Layer Meteorol.* 5:159–75
- McEwan AD, Plumb RA. 1977. Off-resonant amplification of finite internal wave packets. *Dyn. Atmos. Oceans* 2:83–105
- Mercier MJ, Garnier N, Dauxois T. 2008. Reflection and diffraction of internal waves analyzed with the Hilbert transform. *Phys. Fluids* 20:086601
- Mercier MJ, Martinand D, Mathur M, Gostiaux L, Peacock T, Dauxois T. 2010. New wave generation. *J. Fluid Mech.* 657:308–34
- Mied RP. 1976. The occurrence of parametric instabilities in finite-amplitude internal gravity waves. *J. Fluid Mech.* 78:763–84
- Moudjed B, Botton V, Henry D, Ben Hadid H, Garandet JP. 2014. Scaling and dimensional analysis of acoustic streaming jets. *Phys. Fluids* 26:093602
- Mowbray DE, Rarity BS. 1967. A theoretical and experimental investigation of the phase configuration of internal waves of small amplitude in a density stratified fluid. *J. Fluid Mech.* 28:1–16
- Nazarenko S. 2011. *Wave Turbulence*. Berlin: Springer-Verlag
- Nyborg WL. 1965. Acoustic streaming. In *Properties of Polymers and Nonlinear Acoustics*, ed. WP Mason, pp. 265–331. Phys. Acoust. Ser. 2B. San Diego: Academic
- Pairaud I, Staquet C, Sommeria J, Mahdizadeh M. 2010. Generation of harmonics and sub-harmonics from an internal tide in a uniformly stratified fluid: numerical and laboratory experiments. In *IUTAM Symposium on Turbulence in the Atmosphere and Oceans*, ed. D Dritschel, pp. 51–62. IUTAM Bookser. 28. Berlin: Springer-Verlag
- Peacock T, Echeverri P, Balmforth NJ. 2008. An experimental investigation of internal tide generation by two-dimensional topography. *J. Phys. Oceanogr.* 38:235–42
- Phillips OM. 1966. *The Dynamics of the Upper Ocean*. New York: Cambridge Univ. Press
- Plumb RA. 1977. The interaction of two internal waves with the mean flow: implications for the theory of the quasi-biennial oscillation. *J. Atmos. Sci.* 34:1847–58
- Plumb R, McEwan A. 1978. The instability of a forced standing wave in a viscous stratified fluid: a laboratory analogue of the quasi-biennial oscillation. *J. Atmos. Sci.* 35:1827–39
- Rainville L, Pinkel R. 2006. Propagation of low-mode internal waves through the ocean. *J. Phys. Oceanogr.* 36:1220–36
- Riley N. 2001. Steady streaming. *Annu. Rev. Fluid Mech.* 33:43–65
- Sarkar S, Scotti A. 2016. Turbulence during generation of internal tides in the deep ocean and their subsequent propagation and reflection. *Annu. Rev. Fluid Mech.* 49:195–220
- Scolan H, Ermanyuk E, Dauxois T. 2013. Nonlinear fate of internal waves attractors. *Phys. Rev. Lett.* 110:234501
- Semin B, Facchini G, Pétrélis F, Fauve S. 2016. Generation of a mean flow by an internal wave. *Phys. Fluids* 28:096601



- Staquet C, Sommeria J. 2002. Internal gravity waves: from instabilities to turbulence. *Annu. Rev. Fluid Mech.* 34:559–93
- Squires TM, Quake SR. 2013. Microfluidics: fluid physics at the nanoliter scale. *Rev. Mod. Phys.* 77:977–1026
- Sun O, Pinkel R. 2013. Subharmonic energy transfer from the semi-diurnal internal tide to near-diurnal motions over Kaena Ridge, Hawaii. *J. Phys. Oceanogr.* 43:766–89
- Sutherland BR. 2010. *Internal Gravity Waves*. Cambridge, UK: Cambridge Univ. Press
- Sutherland BR. 2013. The wave instability pathway to turbulence. *J. Fluid Mech.* 724:1–4
- Tabaei A, Akylas TR. 2003. Nonlinear internal gravity wave beams. *J. Fluid Mech.* 482:141–61
- Tabaei A, Akylas TR, Lamb KG. 2005. Nonlinear effects in reflecting and colliding internal wave beams. *J. Fluid Mech.* 526:217–43
- Thomas NH, Stevenson TN. 1972. A similarity solution for viscous internal waves. *J. Fluid Mech.* 54:495–506
- van den Bremer TS, Sutherland BR. 2014. The mean flow and long waves induced by two-dimensional internal gravity wavepackets. *Phys. Fluids* 26:106601
- Voisin B. 2003. Limit states of internal wave beams. *J. Fluid Mech.* 496:243–93
- Westervelt PJ. 1953. The theory of steady rotational flow generated by a sound field. *J. Acoust. Soc. Am.* 25:60–67
- Wunsch C, Ferrari R. 2004. Vertical mixing, energy, and the general circulation of the oceans. *Annu. Rev. Fluid Mech.* 36:281–314
- Xie JH, Vanneste J. 2014. Boundary streaming with Navier boundary condition. *Phys. Rev. E* 89:063010
- Young WR, Tsang Y-K, Balmforth NJ. 2008. Near-inertial parametric subharmonic instability. *J. Fluid Mech.* 607:25–49
- Zhou Q, Diamessis PJ. 2013. Reflection of an internal gravity wave beam off a horizontal free-slip surface. *Phys. Fluids* 25:036601

